The 2008 Methoni earthquake sequence: the relationship between the earthquake cycle on the subduction interface and coastal uplift in SW Greece (supplementary material)

Andy Howell, Kirill Palamartchouk, Xanthos Papanikolaou, Demitris Paradissis, Costas Raptakis, Alex Copley, Philip England and James Jackson

Figure 1 shows the source model for the 2013 October 12 M_W 6.5 earthquake (see Section 4.1 of the main paper for details of the inversion procedure).

Figures 2–6 show fit of modelled GPS time series to observations for the model presented in Figure 7 of the main paper.

Table 1 lists elevations of uplifted late-Holocene palæoshorelines used to calculate misfits of models in Appendix B of the main paper.

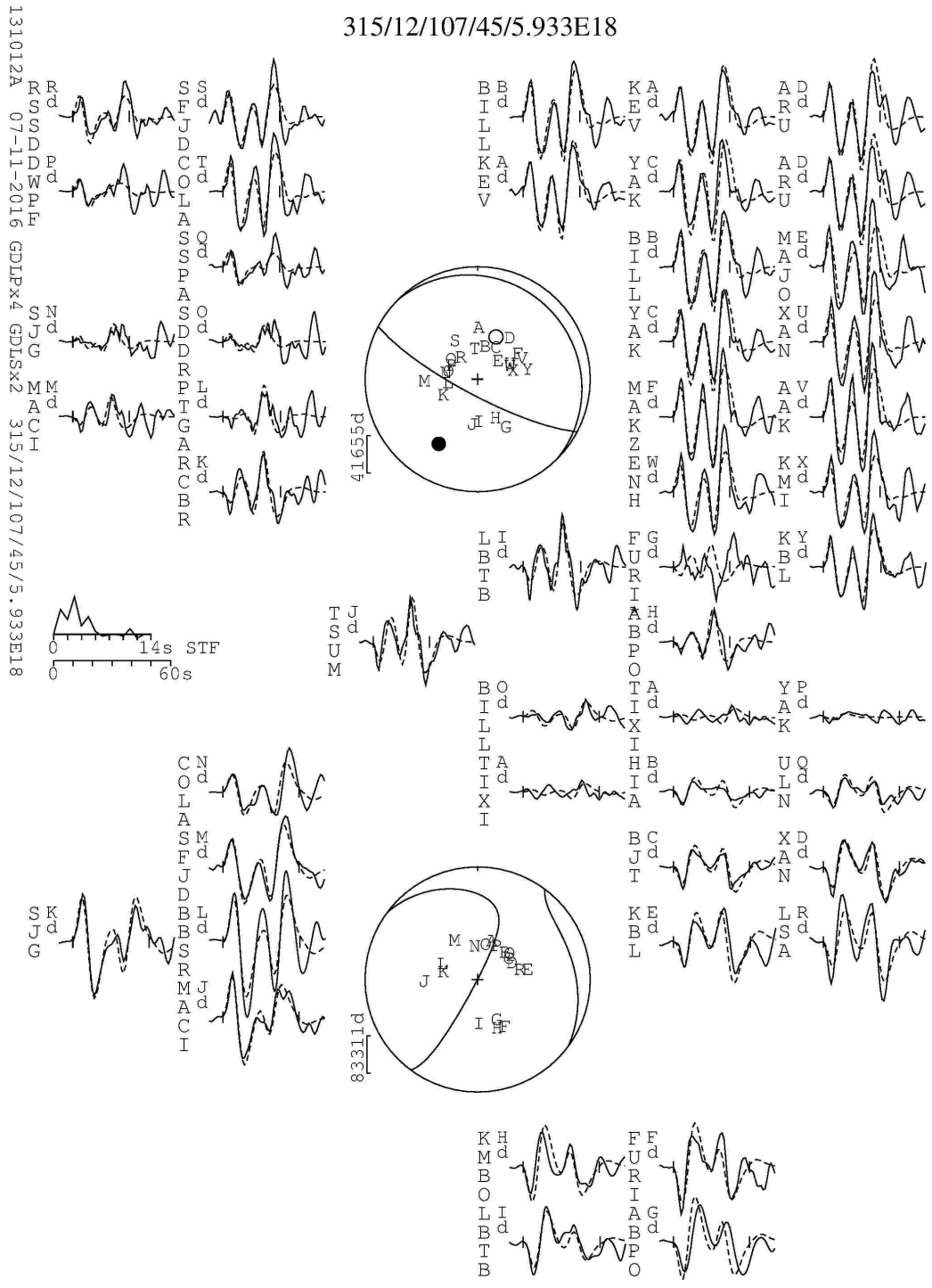

Figure 1: Fit of synthetic to observed waveforms for the 2013 October 12 M_W 6.5 earthquake. The event header (top) shows the strike, dip, rake, centroid depth and scalar seismic moment (in Nm) of the minimum misfit solution. The top focal sphere shows the lower hemisphere stereographic projection of the P-waveform nodal planes, and the positions of the seismic stations used in the inversion. The lower panel shows the *SH* focal sphere. Capital letters next to the station codes correspond to the position on the focal sphere, ordered clockwise by azimuth, starting at north. Solid and dashed lines show the observed and synthetic waveforms respectively. The inversion window is marked by vertical lines on each waveform. The source-time function (STF) is shown, with the time scale for the waveforms below it. The amplitude scales for the waveforms are shown below each focal sphere. The P-and T-axes within the P-waveform focal sphere are shown by a solid and an open circle, respectively.

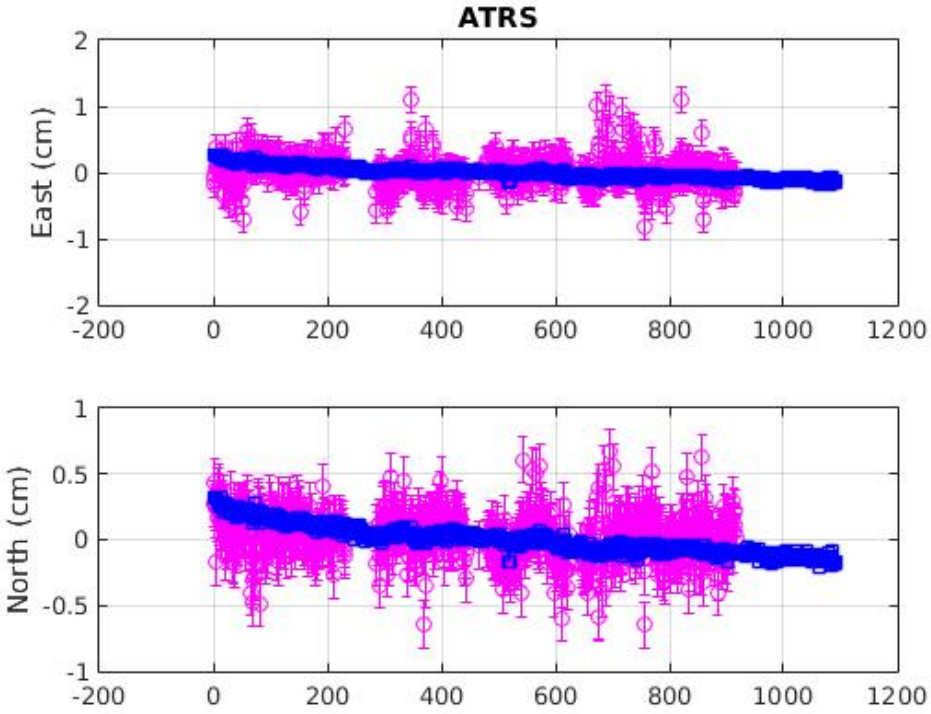

Figure 2: Fit of modelled to observed post-seismic time series at station ATRS (Figure 4, main text). Observations and errors are shown in pink, with modelled displacements in blue. The x-axis is in days after February 14, 2008 (the date of the Methoni earthquakes). Data are centred as part of the PCAIM inversion procedure (Kositsky and Avouac, 2010), so zero on the y-axis does not correspond to the position immediately after the earthquakes.

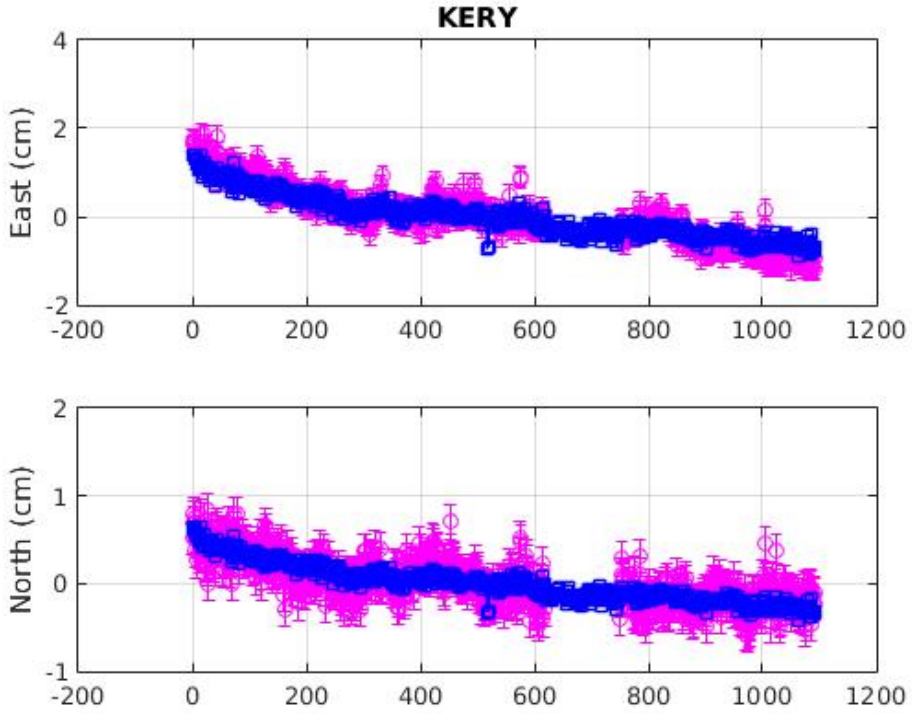

Figure 3: Fit of modelled to observed post-seismic time series at station KERY (Figure 4, main text). Observations and errors are shown in pink, with modelled displacements in blue. The x-axis is in days after February 14, 2008 (the date of the Methoni earthquakes). Data are centred as part of the PCAIM inversion procedure *Kositsky and Avouac* (2010), so zero on the y-axis does not correspond to the position immediately after the earthquakes.

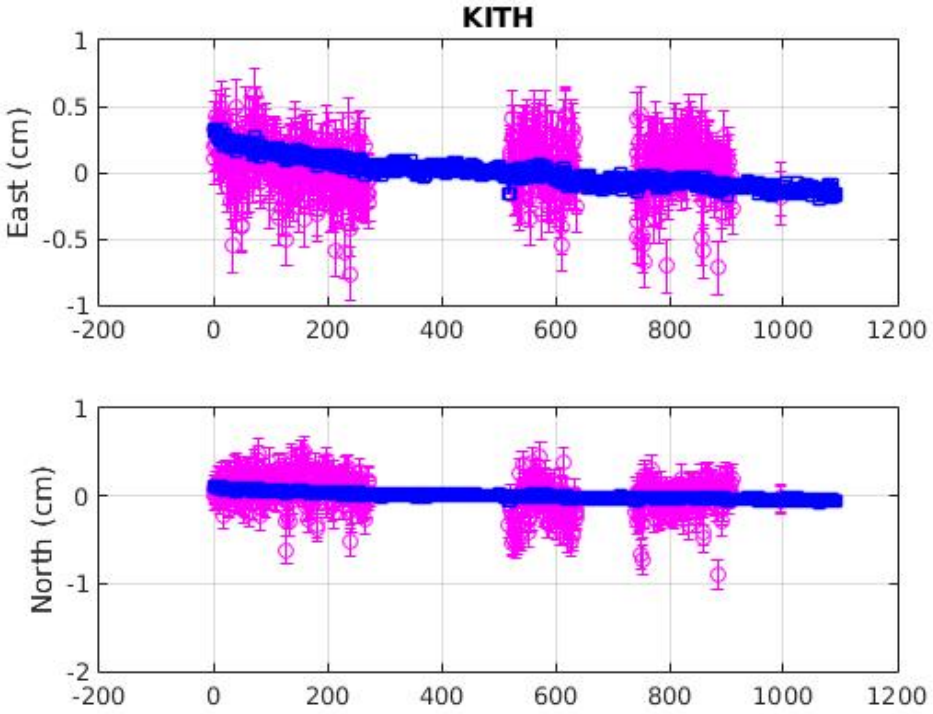

Figure 4: Fit of modelled to observed post-seismic time series at station KITH (Figure 4, main text). Observations and errors are shown in pink, with modelled displacements in blue. The x-axis is in days after February 14, 2008 (the date of the Methoni earthquakes). Data are centred as part of the PCAIM inversion procedure *Kositsky and Avouac* (2010), so zero on the y-axis does not correspond to the position immediately after the earthquakes.

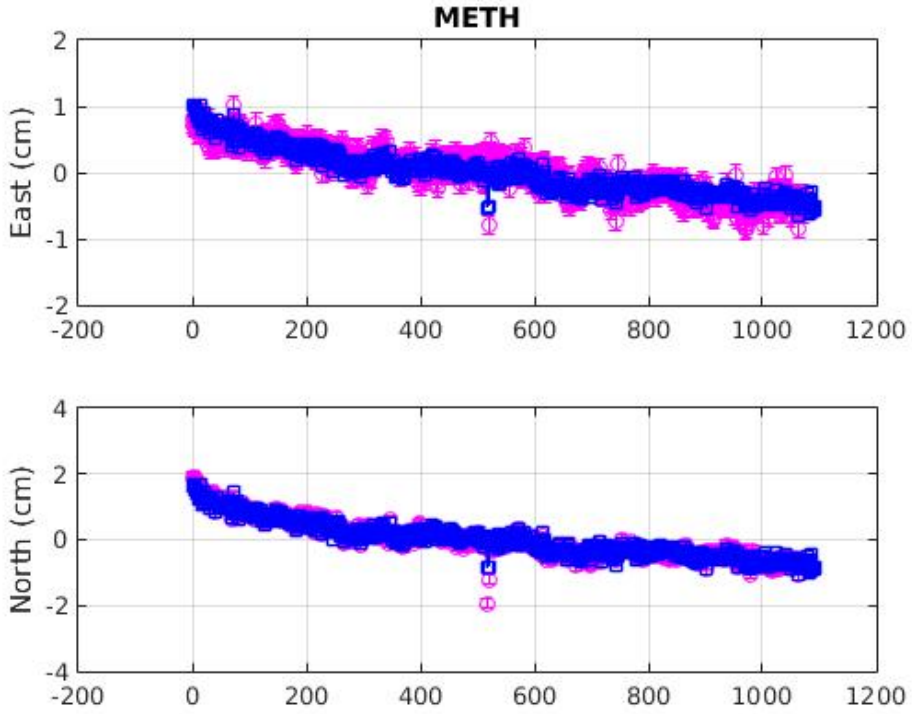

Figure 5: Fit of modelled to observed post-seismic time series at station METH (Figure 4, main text). Observations and errors are shown in pink, with modelled displacements in blue. The x-axis is in days after February 14, 2008 (the date of the Methoni earthquakes). Data are centred as part of the PCAIM inversion procedure *Kositsky and Avouac* (2010), so zero on the y-axis does not correspond to the position immediately after the earthquakes.

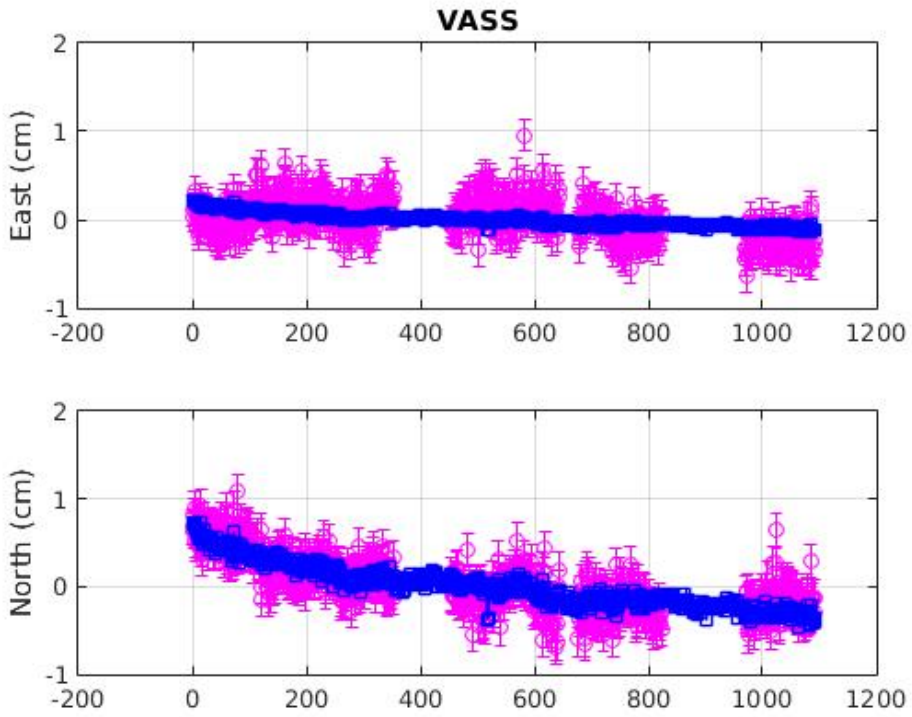

Figure 6: Fit of modelled to observed post-seismic time series at station VASS (Figure 4, main text). Observations and errors are shown in pink, with modelled displacements in blue. The x-axis is in days after February 14, 2008 (the date of the Methoni earthquakes). Data are centred as part of the PCAIM inversion procedure *Kositsky and Avouac* (2010), so zero on the y-axis does not correspond to the position immediately after the earthquakes.

Longitude (°)	Longitude (°)	Elevation (m)
24.401	35.183	2.0
24.414	35.175	2.0
24.479	35.153	1.7
24.565	35.103	1.6
23.777	35.574	4.1
23.726	35.535	5.5
23.602	35.592	6.0
23.787	35.240	7.1
23.637	35.230	9.0
23.962	35.230	5.0
24.267	35.367	1.5
23.933	35.533	3.1
23.600	35.600	5.2
23.567	35.500	6.7
23.550	35.383	7.0
23.533	35.317	7.8
23.817	35.250	7.0
24.017	35.200	4.3
24.017	35.200	4.4
24.067	35.200	3.8
24.100	35.200	3.6
24.400	35.183	1.7
23.267	35.867	2.7
23.283	35.867	2.7
23.283	35.883	2.2
23.317	35.833	2.7
23.317	35.817	2.7
24.041	34.866	0.0
24.100	34.833	0.0

Table 1: Uplift measurements used in the grid searches in Appendix B. Elevations are the height of the highest late-Holocene palæoshoreline above present-day sea level. Measurements are from *Shaw et al.* (2008), *Pirazzoli et al.* (1982) and *Spratt* (1865).

References

Kositsky, A. P., and J.-P. Avouac, Inverting geodetic time series with a principal component analysis-based inversion method, *J. Geophys. Res.*, *115*(B3), B03,401, doi:10.1029/2009JB006535, 2010.

Pirazzoli, P., J. Thommeret, Y. Thommeret, J. Laborel, and L. Montaggioni, Crustal block movements from Holocene shorelines: Crete and Antikythira (Greece), *Tectonophysics*, *86*(1-3), 27–43, doi:10.1016/0040-1951(82)90060-9, 1982.

Shaw, B., et al., Eastern Mediterranean tectonics and tsunami hazard inferred from the AD 365 earthquake, *Nat. Geosci.*, *1*(4), 268–276, 2008.

Spratt, T. A. B., *Travels and Researches in Crete, vol. I, II*, J. van Voorst, London, 1865, 1865.